Nanoscale

Accepted Manuscript

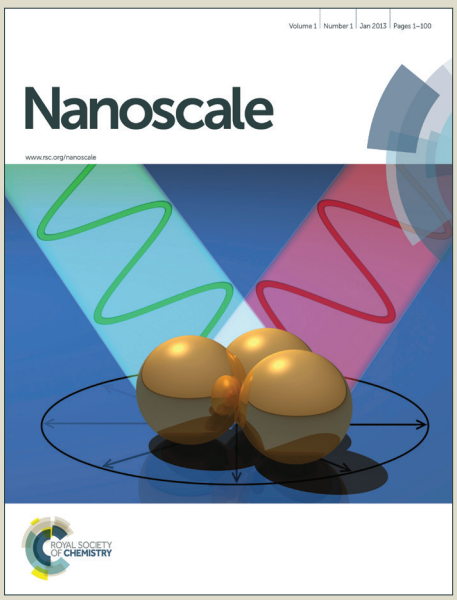

ROYAL SOCIETY OF CHEMISTRY

www.rsc.org/nanoscale

Molecular mechanism of fullerene-inhibited aggregation of Alzheimer's β-amyloid peptide fragment

*Luogang Xie, Yin Luo, Dongdong Lin, Wenhui Xi, Xinju Yang and Guanghong Wei**

[†]State Key Laboratory of Surface Physics, Key Laboratory for Computational Physical Sciences (Ministry of Education), and Department of Physics, Fudan University, 220 Handan Road, Shanghai, 200433, China

***Correspondence to:**

Guanghong Wei, Department of Physics, Fudan University, 220 Handan Road, Shanghai, 200433, China.
Tel: (86) 21 55665231, Email: ghwei@fudan.edu.cn

ABSTRACT: Amyloid deposits are implicated in the pathogenesis of many neurodegenerative diseases such as Alzheimer's disease (AD). The inhibition of β-sheet formation has been considered as the primary therapeutic strategy for the AD. Increasing data show that nanoparticles can retard or promote the fibrillation of amyloid-β (Aβ) peptide depending on the physicochemical properties of nanoparticles, however, the underlying molecular mechanism remains elusive. In this study, our replica exchange molecular dynamics (REMD) simulations show that fullerene

nanoparticle -- C_{60} (with a fullerene:peptide molar ratio greater than 1:8) can dramatically prevent β-sheet formation of Aβ(16-22) peptides. Atomic force microscopy (AFM) experiments further confirm the inhibitory effect of C_{60} on Aβ(16-22) fibrillation, in support of our REMD simulations. An important finding from our REMD simulations is that fullerene C_{180}, albeit with the same number of carbon atoms as three C_{60} molecules ($3C_{60}$) and smaller surface area than $3C_{60}$, displays an unexpected stronger inhibition effect on the β-sheet formation of Aβ(16-22) peptide. A detailed analysis of the fullerene-peptide interaction reveals that the stronger inhibition of β-sheet formation by C_{180} results from the strong hydrophobic and aromatic-stacking interactions of the fullerene hexagonal rings with the Phe rings relative to the pentagonal rings. The strong interactions between the fullerene nanoparticles and Aβ(16-22) peptides significantly weaken the peptide-peptide interaction that is important for β-sheet formation, thus retarding Aβ(16-22) fibrillation. Overall, our studies reveal the significant role of fullerene hexagonal rings on the inhibition of Aβ(16-22) fibrillation and provide novel insight into the development of drug candidates against Alzheimer's disease.

Keywords: fullerene nanoparticle; β-amyloid peptide; pentagonal/hexagonal rings; replica-exchange molecular dynamics simulations; atomic force microscopy.

1. INTRODUCTION

The fast-developing field of nanotechnology has a significant impact on numerous areas of science and technology.[1] Although remarkable developments have been made in nanoscience field, the effects of nanomaterials on biological molecules remain mostly unclear.[2] The understanding of the interactions between nanomaterials and biomolecules are essential to nanoparticle-based biotechnology and biomedical applications, such as gene delivery,[3] cellular imaging,[4] tumor therapy,[5] biological experimental technology,[6] and protein amyloidosis.[7] The amyloid formation of proteins has been received considerable attention due to its close association with many diseases, such as Alzheimer's disease, type II diabetes and Parkinson disease. Increasing experimental studies reported that nanoparticles including carbon nanoparticles,[8-10] polymeric and fluorinated nanoparticles[11, 12], gold nanoparticles[13-16] and inorganic nanoparticles[17] can inhibit/promote amyloid fibril formation depending on their surface physicochemical properties by increasing/decreasing the lag phase time for nucleation, but they all leave the elongation phase invariant, suggesting a nanoparticle-modulated mechanism.[10, 11] The influence of carbon nanoparticles and other type of nanoparticles on protein fibrillation has been attracted considerable attention recently, as reported in two recent reviews.[18, 19] It is fundamental importance to understand the nanoparticle-mediated mechanism of peptide aggregation at atomic details.

Alzheimer's disease (AD) is the most common neurodegenerative disorder with senile plaques constituted by amyloid-β (Aβ) protein in patients' brain tissues.[20] Aβ

□is a 39-42-residue peptide and its pathological aggregation can lead to the formation of insoluble amyloid fibrils. Amyloid fibrils display a cross-β structure with the β-strands perpendicular to and the inter-strand hydrogen bonds parallel to the fibril axis.[21-23] The formation of amyloid fibril has been proposed to follow a two-step kinetics process (nucleation-elongation), which is characterized by a long lag phase associated with the formation of a nucleus followed by a rapid fibril elongation.[24] These amyloid fibrils have been considered to be the disease agents, but increasing evidence suggests that small oligomers formed in the early stage of nucleation process are the most cytotoxic species in neurodegenerative diseases.[25, 26] However, these soluble oligomers are difficult to characterize experimentally due to their transient and polymorphic nature. An understanding of the structure of the amyloid oligomers at atomic resolution and the factors that influence peptide aggregation is crucial for the rational design of novel therapeutic strategies.

Carbon nanoparticles are one of the most prevalent types of nanomaterials present in the environment, whose dimensions are within 1-100 nm. Fullerenes, such as C_{60} and C_{180}, are small carbon nanoparticles with spherical cage shape. Increasing experimental studies[8, 27-31] indicate that fullerene and its derivatives have remarkable anti-amyloid properties for Alzheimer's disease and other neurodegenerative diseases. Using ThT fluorescence measurements, Kim and Lee studied the effect of 1,2-(dimethoxylmethano)fullerene on the fibrillation of Aβ(1-40) and the 11-25 fragment of Aβ and suggested that this modified fullerene can specifically bind to the central hydrophobic motif KLVFF, therefore suppressing Aβ fibrillation.[8] By using

transmission electron microscopy (TEM) measurements, Podolski et al.[27 28] proposed that hydrated fullerene (C_{60}:$(H_2O)_n$) inhibited the fibril formation of Aβ(25-35) peptide. More complicated derivatives of fullerenes such as $C_{60}Cl(C_6H_4CH_2COONa)$, $Na_4[C_{60}(OH)_{\sim 30}]$ and the complexes of fullerene with polyvinylpyrrolidone, were reported to prevent the fibrillation and cytotoxicity of Aβ(1-42).[29-31] Computationally, using docking method and conventional molecular dynamics simulations, Andujar et al examined the influence of pristine of C_{60} on the structural stability of a constructed fibril-like Aβ(1-42) pentamer and reported that C_{60} preferentially bound to the core part of the fibril and destabilized the fibril structure.[32] These experimental and computational studies have greatly enhanced our understanding of the impact of the fullerenes on the aggregation of Aβ and its Aβ(25-35) fragment, however, the inhibition mechanism as well as the effects of concentration and fullerene nanoparticle size on the structures of Aβ oligomeric species remain elusive.

It was proposed that the central hydrophobic core (CHC) Aβ(17-20), i.e. LVFF, is essential for β-sheet formation of full-length Aβ.[33] The Aβ(16-22) fragment (with amino acid sequence KLVFFAE), containing this CHC, is among the shortest sequences that form amyloid fibrils similar to Aβ □fibrils at neutral pH.[34] Thus, Aβ(16-22) is an ideal candidate for studying the molecular mechanism of nanoparticle-mediated aggregation of Aβ□ peptide. In this work, we studied the octamerization of Aβ(16-22) peptide in the presence of C_{60} and C_{180} nanoparticles by performing extensive replica-exchange molecular dynamics (REMD) simulations with explicit water. The reason of choosing an octamer is that previous all-atom MD

studies indicated that the minimum nucleus size consists of at least eight Aβ(16-22) peptide chains based on the stability of preformed β-sheet assemblies.[35] We first examine the influence of C_{60} concentration on Aβ(16-22) aggregation by performing REMD simulations on Aβ(16-22) octamers in the presence of one or three C_{60} molecules. Our simulations show that fullerene C_{60} (with a fullerene:peptide molar ratio greater than 1:8) can significantly prevent β-sheet formation of Aβ(16-22) peptide. Atomic force microscopy (AFM) experiments provide evidence demonstrating the inhibitory effect of C_{60} on Aβ(16-22) fibrillation. Then we investigate the size effect of fullerene nanoparticles on Aβ(16-22) self-assembly by conducting REMD simulations on Aβ(16-22) octamers in the presence of a bigger fullerene nanoparticle -- C_{180}. Fullerene C_{180} has an identical number of carbon atoms with three C_{60} (denoted by $3C_{60}$) molecules, but smaller surface area, which is expected to have a lower probability to interact with Aβ(16-22) peptide and lead to weaker inhibition effect on β-sheet formation. Surprisingly, our REMD simulations reveal that fullerene C_{180} displays stronger inhibition effect on β-sheet formation than $3C_{60}$. Analyses of the fullerene-peptide interaction reveal that this stronger β-sheet inhibition effect results from the stronger hydrophobic and aromatic-stacking interactions between fullerene hexagonal rings and Phe rings. To the best of knowledge, this is the first report to investigate the molecular mechanism of fullerene-inhibited aggregation of Aβ(16-22) using extensive REMD simulations.

2. MATERIALS AND METHODS

Aβ(16-22)-fullerene systems. Three systems have been studied: Aβ+C_{60}, Aβ+$3C_{60}$,

and Aβ+C_{180}. Here, for brevity, we use Aβ□ for□ Aβ(16-22). The Aβ(16-22) peptide consists of seven amino acid residues (Ac-KLVFFAE-NH_2) and is capped by acetyl and amine groups as determined experimentally.[34] To mimic the experimental neutral pH condition, the side chain of Lys is protonated (Lys^+) and that of Glu is deprotonated (Glu^-). The eight peptide chains in the initial state of Aβ(16-22) octamer have random character, similar to those in our previous study.[36] The C_{60}, $3C_{60}$ and C_{180} are randomly dispersed in the peptide system. The initial states of the three systems are given in Fig. S1. Each system was placed in a cubic box (6.8 × 6.8 × 6.8 nm^3) of SPC water molecule[37] with a minimum distance of 0.9 nm to the water box wall. The total numbers of atoms for the three systems are 30250, 30361 and 28270, respectively.

REMD simulations. Three 200-ns REMD[38] simulations were performed using the GROMACS-4.5.3 software package.[39, 40] We chose the GROMOS96 43a1 force field[41] in accordance with previous computational studies of Aβ(16-22).[36, 42-44] To avoid high-pressure artifacts at elevated temperature, we carried out REMD simulations in the NPT ensemble at a pressure of 1 bar. There are 40 replicas, each of 200 ns duration, at temperatures exponentially spaced between 310 K and 420 K. The carbon atoms of fullerenes (C_{60} and C_{180}) were uncharged in accordance with our previous studies.[36, 45]

Our in-home-developed codes and the facilities implemented in the GROMACS software package were used for the trajectory analysis. We discarded the first 60 ns of each REMD run to remove the bias of the initial states; therefore, the structural

properties of each system were based on the simulation data generated in the last 140 ns. We analyzed the REMD trajectories using several parameters, including the secondary structure content, the free energy landscape (or potential of mean force), the percentage of various sizes of β-sheets, the number of hydrogen bonds (H-bonds), the connectivity length (CL), the configuration type (CT), the probability of residue-residue contacts, the Aβ-fullerene contact surface area, the probability density function (PDF) of the distance between the centroids of Phe ring and its closest carbon rings of fullerene, and the PDF of the angle between the two rings. A detailed description of these parameters is given in the Supporting Material. All representations of the studied systems are drawn using the VMD program.[46]

The binding energy (in units of kcal/mol) of fullerenes ($3C_{60}$ and C_{180}) with Aβ(16-22) octamer is estimated by using the Molecular Mechanics/Generalized Born Surface Area (MM/GBSA) method as implemented in AMBER package[47]. This approach is computationally less expensive than free energy perturbation and thermodynamic integration methods as it consider only the unbound and bound states. In MM/GBSA, the binding free energy (ΔG_{bind}) between a ligand and a receptor is calculated as, $\Delta G_{bind} = \Delta E_{MM} + \Delta G_{sol} - T\Delta S$. Here, ΔE_{MM} contains an intermolecular electrostatic term (ΔE_{ele}), a van der Waals (vdW) term (ΔE_{vdW}), and a bonded energy term (ΔE_{bonded}: bond, angle, and dihedral energies). In this study, the carbon atoms of fullerenes (C_{60} and C_{180}) were uncharged, thus the electrostatic term (ΔE_{ele}) is zero. ΔG_{sol} is the sum of polar solvation energy, ΔG_{GB}, and nonpolar solvation component ΔG_{surf}. ΔG_{GB} is calculated by GB model[48], and ΔG_{surf} is estimated by solvent

accessible surface area (SASA). The binding free energy (ΔG_{bind}) reported here is the relative binding free energy, where contribution from conformational entropy of the peptides was frequently neglected.[49-51]. So, the binding energy is estimated by $\Delta G_{bind} = \Delta E_{vdW} + \Delta G_{GB} + \Delta G_{surf}$.

AFM experiments. Synthetic Aβ(16-22) peptides (Ac-KLVFFAE-NH_2) were purchased from GL Biochem (Shanghai) Ltd. They were further purified by high performance liquid chromatography (HPLC) to reach the purity of greater than 98 %. Fullerene C_{60} (purity > 99.9 %) was purchased from XF Nano INC (Nanjing). The peptide solution was prepared by dissolving Aβ(16-22) in deionized water (18.2 MΩ·cm), with a concentration of 0.05 mM. Water-miscible C_{60} was prepared by mixing 3.6 mg C_{60} with 100 mL water and applied with an ultrasonic bath for one hour at a temperature of 60 °C. To investigate the effect of C_{60} on the aggregation of Aβ, Aβ+C_{60} mixed solutions with a C_{60}:Aβ molar ratio of 1:5 and 3:5 were prepared by adding C_{60} aqueous solution into freshly prepared Aβ(16-22) solution. The prepared solutions were fully mixed with ultrasonic bath in ice-cooled water for one minute. All of the solutions were incubated at 37 °C in a hygrothermostat without stirring. The detailed description of AFM imaging of Aβ(16-22) aggregation in the absence and presence of C_{60} nanoparticles is given in the Supporting Material.

3. RESULTS AND DISCUSSION

Three 200-ns REMD runs were performed on the three systems: Aβ+C_{60}, Aβ+3C_{60} and Aβ+C_{180}. The convergences of the three REMD runs were verified by comparing

the probability density function (PDF) of end-to-end distance of each chain and the secondary structure contents (including coil, β-sheet, β-bridge and bend) of Aβ(16-22) within two different time intervals using the 60-130 ns and 130-200 ns data. We also check the sampling efficiency by following the time evolution of temperature swapping of one representative replica in temperature space. As shown in Fig. S1(d-f), the distributions of end-to-end distance within the two independent time intervals overlap very well for Aβ(16-22) peptides in the three systems. The time evolution of a representative replica (Figure S1(g)-(i)) indicates that each Aβ(16-22)−fullerene system sufficiently visited the whole temperature space. Other replicas show similar behavior (data not shown). The residue-based secondary structure contents are almost the same between the two time intervals (Figure S2), with differences within 0.2 % ~ 6.3 %. These data suggest that our REMD simulations for the three systems are reasonably converged.

Fullerenes $3C_{60}$ and C_{180} significantly reduce β-sheet content. We have examined the structural properties of Aβ(16-22) octamers in the three different Aβ-fullerene systems at 310 K. Overall, Aβ(16-22) peptides populate different secondary and tertiary structures in the three systems (see below for more detailed description).

Table 1: Secondary structure probabilities of Aβ(16-22) octamers with and without fullerene nanoparticles.

Systems	Coil (%)	β-sheet (%)	β-bridge (%)	Bend (%)
Aβ‡	50.7 ± 4.1	44.5 ± 3.7	3.0 ± 0.7	1.4 ± 0.6
Aβ+C60	50.9 ± 3.6	45.2 ± 3.2	2.6 ± 0.3	1.2 ± 0.2

Aβ+3C60	67.9 ± 4.8	25.7 ± 1.8	3.8 ± 0.4	2.3 ± 0.5
Aβ+C180	76.0 ± 6.8	18.1 ± 2.1	2.7 ± 0.6	2.4 ± 0.5

‡Data refer to Aβ(16-22) octamer without fullerenes in a 110-ns REMD simulation.[36] For brevity, we use Aβ for Aβ(16-22).

Table 1 gives the secondary structure (coil, β-sheet, β-bridge and bend) percentage averaged over all residues of Aβ(16-22) octamer in the absence and presence of fullerene nanoparticles. The data for Aβ(16-22) without fullerenes are from our previous study.[36] Note that the turn and helix contents are negligible (data not shown). As can be seen from Table 1, coil and β-sheet contents are dominant but they are quite different in the four different systems. We notice that the percentages of each secondary structure composition are almost the same for Aβ in isolation and in Aβ+C_{60} complex, indicating that fullerene C_{60} at low concentration (with a 1:8 molar ratio of C_{60} to Aβ) hardly impacts the aggregation of Aβ(16-22). When the number of C_{60} increases to three (with a 3:8 molar ratio of C_{60} to Aβ), we find that β-sheet content has a considerable decrease from 44.5 % (without C_{60}) to 25.7 % (with $3C_{60}$) and the coil increases rapidly from 50.7 % to 67.9 %. These results indicate that fullerene C_{60} can significantly inhibit β-sheet formation of Aβ when the molar ratio of C_{60}:Aβ is greater than 1:8. When the three C_{60} molecules are replaced by one C_{180} molecule (C_{180} has the same number of carbon atoms as $3C_{60}$), Aβ displays a dramatically reduced β-sheet content of 18.1 %. It should be noted that the simulation time of REMD run for Aβ without nanoparticle was 110 ns in our previous work.[36] When we extended the REMD simulation to 200 ns, the β-sheet content increased

from 44.5 % to 46.6 %, slightly higher than the β-sheet content of 45.2 % in Aβ+C_{60} system. As the Aβ(16-22) octamer in isolation and in Aβ+C_{60} complex has a comparable secondary structure propensity, in the following sections of the manuscript, we take the Aβ(16-22) in Aβ+C_{60} complex as a reference to investigate the effect of higher concentration of C_{60} and the large size of fullerene C_{180} on the octamerization of Aβ(16-22) peptide.

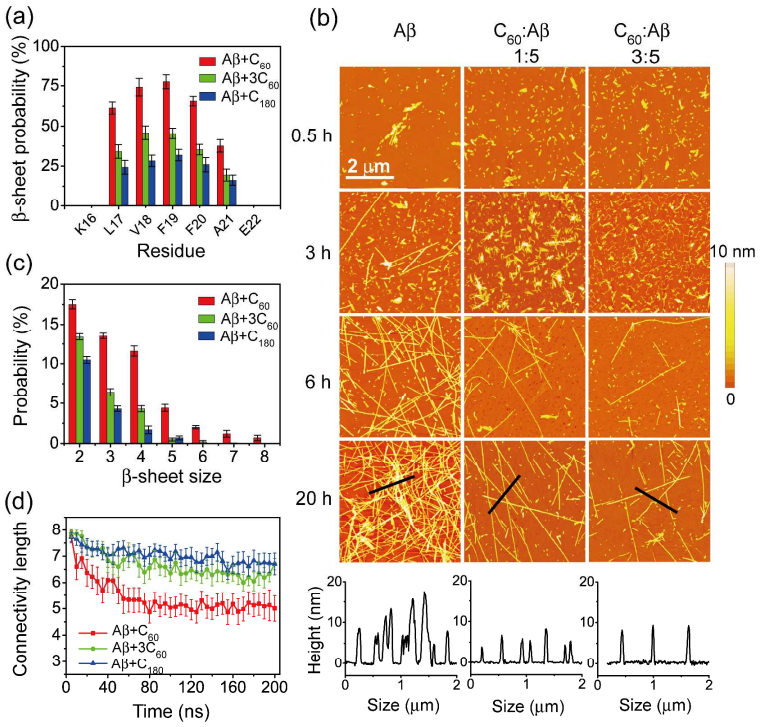

Figure 1: Calculated β-sheet probability of each residue (a), probability of different sizes of β-sheet (c) and the time evolution of connectivity length (CL) (d) of the Aβ(16-22) octamers in Aβ+C_{60}, Aβ+3C_{60} and Aβ+C_{180} systems at 310 K. AFM images (upper panel in (b)) of Aβ(16-22) aggregates with/without C_{60} nanoparticles at four different co-incubation time points and height analysis (bottom panel of (b)) of Aβ(16-22) aggregates incubated at 20 h.

We then calculate the β-sheet percentage of each amino acid residue of Aβ(16-22) peptide in the three different systems and the results are presented in Fig. 1(a). In

Aβ+C_{60} system, residues L17-V18-F19-F20-A21 in the CHC region have 38.7 ~ 78.4 % probabilities to adopt β-sheet conformation, with V18 and F19 having a high β-sheet probability of 75.6 % and 78.4 %. However, in Aβ+3C_{60} system, this region has a distinctly reduced β-sheet probability of 20.9 ~ 46.3 %, with a probability of 41.2 % for V18 and 46.3 % for F19. These results demonstrate that C_{60} nanoparticle with a C_{60}:Aβ molar ratio > 1:8 can significantly inhibit the β-sheet formation of Aβ(16-22) peptides.

To further examine the inhibitory effect of C_{60} on Aβ(16-22) fibrillation and to validate the selected force field, we performed AFM imaging of Aβ(16-22) aggregates with and without C_{60} at four different co-incubation time points (Fig. 1(b)). We see that in the absence of C_{60} (Fig. 1(b) (left)), both small and large aggregates are observed at t = 0.5 h. With the elongation of incubation time, short fibrils appear at t = 3 h and grow into long fibrils at t = 6 h. Significant amount of fibrils are observed at t = 20 h. In the densest region of fibrils, the height of fibrils is varied between 4.8 ~ 17.5 nm, and nine peaks are observed within a width of 2 μm. With the addition of C_{60} (with a C_{60}:Aβ molar ratio 1:5 (> 1:8)), fibrils are not seen within the initial 3 hours. The AFM images taken at co-incubation time of 6 h and 20 h show that the amount of fibrils decrease dramatically (Fig. 1(b) (middle)), compared with that without C_{60} nanoparticles. When the C_{60} concentration is increased to a C_{60}:Aβ molar ratio of 3:5, the inhibitory effect of fibril formation becomes more pronounced as seen from Fig. 1(b) (right). Both the fibril height and the number of fibrils in the presence of C_{60} are reduced relative to the case without C_{60} (bottom panel in Fig. 1(b)). These

AFM results demonstrate that C_{60} can significantly inhibits the fibrillation of Aβ(16-22) peptides (with a C_{60}:Aβ molar ratio > 1:8), in support of our simulation results, indicating the GROMOS96 43a1 force field is appropriate for Aβ(16-22)-fullerene system and the results from our REMD simulations are reliable.

In the presence of C_{180} -- a larger size of fullerene nanoparticle, we found the Aβ(16-22) octamer has the lowest percentage of β-sheet (18.1 %) and the highest percentage of coil (76.0 %) (Table 1). Strikingly, the residues in CHC region have a dramatically reduced β-sheet probability (16.8-32.9 %), with V18 and F19 having respectively a probability of 29.4 and 32.9 % (Fig. 1(a)). The results in Table 1 and Fig. 1(a) illustrate that C_{180} has a pronounced inhibitory effect on the β-sheet formation of Aβ(16-22) peptides.

The effect of fullerene nanoparticles on Aβ(16-22) aggregation is also illustrated by the probability of the β-sheet sizes at 310 K (Fig. 1(c)). In Aβ+C_{60} system (with a C_{60}:Aβ molar ratio of 1:8), we find that the two-, three-, and four-stranded β-sheets have a probability of 17.5 %, 13.5 %, and 11.6 %, respectively. When the C_{60}:Aβ molar ratio is increased to 3:8 (Aβ+3C_{60} system), the populations of these β-sheets are reduced to 13.4 %, 6.4 %, and 4.3 %, respectively. In the system with a larger size of fullerene C_{180} molecule (Aβ+C_{180} system), the percentages of two-, three-, and four-stranded β-sheets are reduced respectively to 10.5 %, 4.3 %, and 1.7 %. Differences are more pronounced for larger sizes of β-sheets. The probabilities of five-, six-, seven-, and eight-stranded β-sheets are respectively 4.4 %, 2.0 %, 1.2 % and 0.7 % in Aβ+C_{60} system, whereas they drop significantly to 0.5 %, 0.2 %, 0.1 %

and 0.0 % in Aβ+3C_{60} system. Strikingly, in Aβ+C_{180} system, these β-sheets almost vanish. These data indicate that the 3C_{60} and C_{180}, especially C_{180}, significantly reduce the populations of all sizes of β-sheets of Aβ(16-22) octamers.

We further probe the ordering of Aβ(16-22) octamers in the presence of C_{60}, 3C_{60} and C_{180} nanoparticles by monitoring the time evolution of the connectivity length (CL) at 310 K (Fig. 1(d)). The CLs of the Aβ(16-22) octamer in these three systems decrease rapidly from the initial value of 7.9 respectively to 5.0, 6.7 and 7.0 within the first 60 ns of the simulations. The CLs during 60-200 ns in the three systems fluctuate around these three values, indicating the three systems have reached equilibrium. Distinct differences for CL are observed among these three systems: larger CL values of 6.7 (in Aβ+3C_{60} system) and 7.0 (in Aβ+C_{180} system) reveal the disordered nature of Aβ(16-22) octamer, reflecting the inhibitory effects of 3C_{60} and C_{180} on the β-sheet formation of Aβ(16-22) peptides.

Interactions of 3C_{60} and C_{180} with Aβ(16-22) peptides shift the population of β-sheet-rich octamers toward disordered aggregates and remarkably alter the free energy landscape of Aβ(16-22) octamer. To investigate the influence of 3C_{60} and C_{180} on the atomic structures of Aβ(16-22) octamers, we performed a chain-independent RMSD-based cluster analysis for 70,000 conformations sampled for the replica at 310 K. Using a C_α-RMSD cutoff of 0.3 nm, the conformations of Aβ(16-22) octamers in Aβ+C_{60}, Aβ+3C_{60}, Aβ+C_{180} systems are separated into 106, 114 and 160 clusters, respectively. The centers of the first six most-populated clusters and their populations are shown in Fig. 2(a-c). These clusters represent 40.5 %,

36.3 % and 35.7 % of all conformations of Aβ(16-22) octamers in Aβ+C_{60}, Aβ+3C_{60} and Aβ+C_{180} systems, respectively. In the presence of a single C_{60}, the clusters in Fig. 2(a) display various ordered and disordered β-sheet-rich conformations. The first and fifth clusters (C1 and C5) contain five- and seven-stranded (CT = 5+3, 7+1) open/closed β-barrels with mixed parallel-antiparallel β-strand alignment, and have a population of 8.9 % and 5.1 %, respectively. C3 and C4 contain parallel β-sheet bilayers (CT = 5+3 and 4+4), with a population of 7.6 % and 7.4 %, respectively. C2 and C6 mainly consist of disordered β-sheet-rich aggregates. In the presence of 3C_{60} and C_{180}, as shown in Fig. 2(b) and (c), Aβ(16-22) octamers are mostly in amorphous states, consisting of mostly random chains as well as two-, three- and four-stranded β-sheets, while ordered structures including bilayer β-sheets and β-barrels are not observed. The Aβ(16-22) octamer in Aβ+C_{180} system appear to be more disordered than that in Aβ+3C_{60} system. These results demonstrate that 3C_{60} and C_{180} shift the population of Aβ(16-22) octamers from β-sheet-rich octamers to coil-rich aggregates.

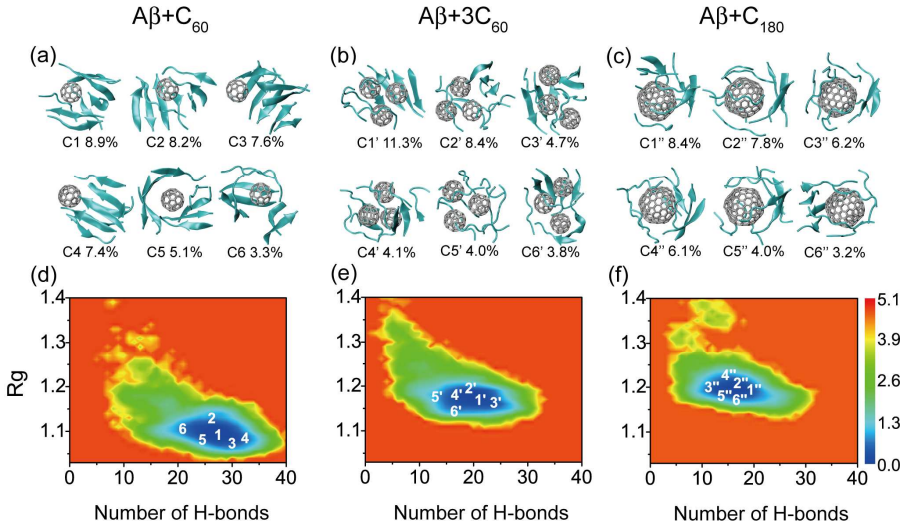

Figure 2: Structure analysis and potential of mean force (PMF) for Aβ(16-22) octamers in

aqueous solution in the presence of C_{60}, $3C_{60}$ and C_{180} nanoparticles. Representative structures for the top six most-populated clusters of Aβ(16-22) octamers in Aβ+C_{60} (a), Aβ+$3C_{60}$ (b) and Aβ+C_{180} (c) systems. The PMF (in kcal/mol) of Aβ(16-22) octamers plotted as a function of the number of intermolecular H-bonds and Rg of the Aβ(16-22) octamers in Aβ+C_{60} (d), Aβ+$3C_{60}$ (e) and Aβ+C_{180} (f) systems.

To have an overall view of the conformational distribution of Aβ(16-22) octamers in the presence of C_{60}, $3C_{60}$ and C_{180} nanoparticles, we plot in Fig. 2(d-f) the potential of mean force (PMF) as a function of the number of intermolecular hydrogen bonds (H-bonds) and the radius of gyration (Rg) of the Aβ(16-22) octamer. The locations of the first six clusters are labeled on the PMF plot. The free energy surfaces of Aβ(16-22) octamers in the three systems display a quite similar shape, while their minimum energy basins are located at different (Number of H-bonds, Rg) values of (28, 1.00), (20, 1.17) and (16, 1.20). Compared with the Aβ(16-22) octamers in Aβ+C_{60} system, Aβ(16-22) octamers in Aβ+$3C_{60}$ and Aβ+C_{180} systems have a decreased number of H-bonds and an increased value of Rg, implying that the presence of $3C_{60}$ and C_{180} induce Aβ(16-22) octamers to form disordered aggregates.

$3C_{60}$ and C_{180} nanoparticles destroy the hydrophobic and aromatic stacking interactions that is important for β-sheet formation of Aβ(16-22) peptides. In order to reveal the dominant residue-residue interactions that affect the β-sheet formation of Aβ(16-22) peptides in the presence of $3C_{60}$ and C_{180} nanoparticles, we plot in Fig. 3 the inter-peptide main chain - main chain (MC-MC) and side chain - side chain (SC-SC) contact probabilities between all pairs of residues. The residue-residue contact probability maps for these three systems display distinct

MC-MC and SC-SC interaction patterns, implying that the nanoparticles significantly impact the inter-peptide interactions. Figure 3(a) and (b) shows that Aβ(16-22) octamers in the presence of a single C_{60} are essentially stabilized by MC-MC interactions of F19-F19 (with a contact probability of 11.2 %), F19-V18 (10.3 %), and F19-L17 (10.2 %) pairs and by SC-SC interactions of F19-F19 (16.6 %), F19-L17 (12.7 %), and F19-F20 (11.0 %) pairs. It is noted that F19-F19 pair has the highest SC-SC contact probabilities, reflecting its important role in the aggregation of Aβ(16-22) peptides, consistent with previous computational and experimental studies.[44, 52, 53] Numerous studies reported that the hydrophobic and aromatic residue Phe plays an important role on the formation and stabilization of amyloid fibrils. For example, proline scanning mutagenesis demonstrated that the aromatic residues at positions 19 and 20 in the CHC region are particularly sensitive to replacement,[52] which makes this region become a prime target in the design of inhibitors.[54, 55] Using X-ray fiber/powder diffraction, Inouye et al.[53] proposed that in the assemblies of wild-type Aβ(16-22) the F19 was involved in hydrophobic contact with amino acids across the intersheet space, whereas the F20 side chain was localized near the slab surface. The relative high MC-MC contact probabilities along the left-diagonal of contact map in Fig. 3(a) indicate that Aβ(16-22) peptides are aligned predominantly in antiparallel orientation, which is quite similar to the β-strand alignment in Aβ(16-22) octamers in aqueous solution without nanoparticle.[36] This is consistent with previous experiment results that in-register antiparallel pattern is the main alignment of β-strands for Aβ(16-22) peptides at pH around 7.0.[34]

When the number of C_{60} is increased to three, we find that although the peptides still adopt mainly antiparallel alignment, the MC-MC contact probabilities are dramatically reduced (6.3 %, 6.6 % and 6.4 % for F19-F19, F19-V18 and F19-L17, respectively) (Fig. 3(c)). For SC-SC interactions (Fig. 3(d)), reduced contact probabilities are also observed with respect to Fig. 3(b), with a contact probability of 12.6 % versus 16.6 % for F19-F19 pair, 11.2 % versus 12.7 % for F19-L17 pair and 6.7 % versus 11.0 % for F19-F20 pair. As for Aβ+C_{180} system in Fig. 3(e) and (f), we find that MC-MC contacts along the left-diagonal of contact map showed the lowest probability (Fig. 3(e)), 5.1 % for F19-F20 pair and 5.2 % for V18-V18 pair. Similarly, relatively lower contact propensities are observed in SC-SC contact map (9.8 %, 8.8 % and 7.4 % for F19-F19, F19-L17 and L17-L17, respectively) (Fig. 3(f)). Overall, fullerene nanoparticles significantly weaken the residue-residue interactions, especially the residue pairs that are critical for β-sheet and fibril formation.

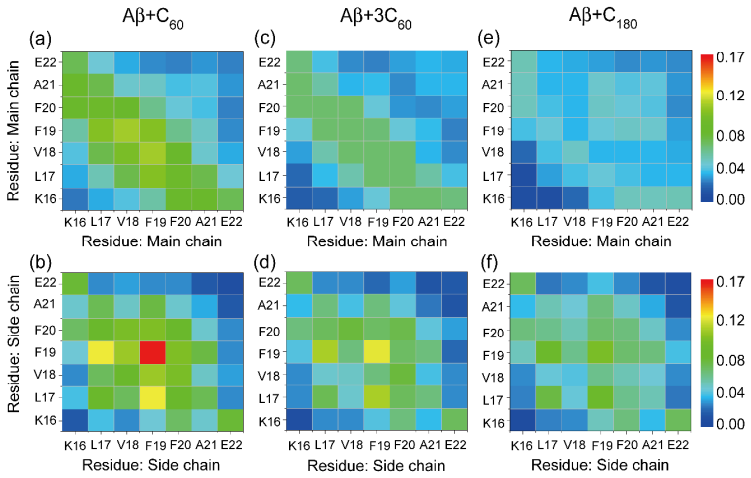

Figure 3: MC-MC and SC-SC contact probability maps for Aβ(16-22) octamers in the presence of C_{60} (a, b), $3C_{60}$ (c, d) and C_{180} (e, f) nanoparticles at 310 K.

The contact surface area between fullerenes and Aβ(16-22) octamers is an important factor that affects the Aβ-fullerene interaction and large contact areas usually imply strong interactions. We plot in Fig. 4(a) the Aβ-fullerene contact surface area in the three systems. Larger Aβ-fullerene contact surface areas are seen in Aβ+3C_{60} and Aβ+C_{180} system relative to the Aβ+C_{60} system. As expected, the Aβ-fullerene interaction in Aβ+3C_{60} and Aβ+C_{180} systems is much stronger than that in Aβ+C_{60} system (red curve in Fig. 4(b)). It can be seen that the Aβ–3C_{60} contact area is slightly larger than that of Aβ–C_{180} (Fig. 4(a)) as 3C_{60} molecules have larger surface area (6.06π nm^2) than a single C_{180} molecule (5.76π nm^2). Unexpectedly, we found that that the Aβ–C_{180} interaction is stronger than Aβ–3C_{60} interaction (red curve in Fig. 4(b)) (see below for more detailed description). This stronger Aβ-C_{180} interaction would interfere with Aβ-Aβ interaction, thus weakening the Aβ-Aβ interaction (black curve in Fig. 4(b)) and inhibiting the β-sheet formation.

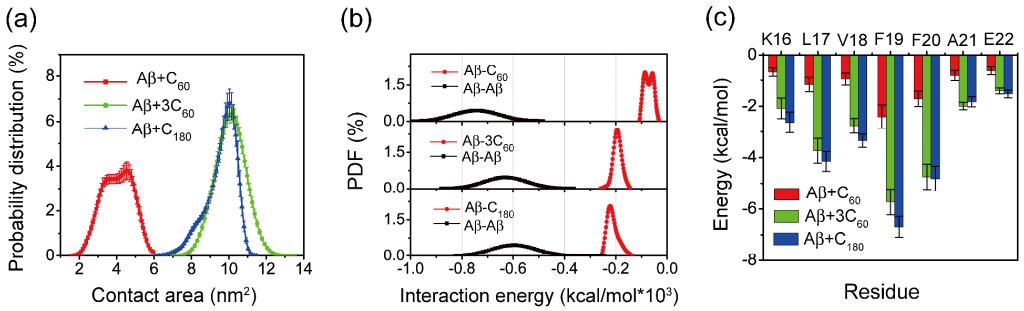

Figure 4: Analysis of Aβ-fullerene interactions in Aβ+C_{60}, Aβ+3C_{60} and Aβ+C_{180} systems at 310 K. (a) The probability distribution of contact surface area, (b) probability density function (PDF) of the different interaction energy terms including Aβ-Aβ and Aβ-fullerene, and (c) the interaction energy of each individual residue of Aβ(16-22) with C_{60}, 3C_{60} and C_{180} nanoparticles.

We also estimate the binding free energy and its components between fullerenes

($3C_{60}$ and C_{180}) and Aβ(16-22) octamer using the MM/GBSA method for the top six most-populated clusters in Aβ+$3C_{60}$ (Fig. 2b) and Aβ+C_{180} (Fig. 2c) systems at 310 K (see Table 2). The binding energy components show that, in comparison with other energy terms, the van der Waals interaction (ΔE_{vdW}) has a dominant contribution to the total binding energy. The strong hydrophobicity of fullerenes leads to the positive value of $\Delta G_{GB} + \Delta G_{surf}$ (solvent effect), indicating that water is unfavorable for the fullerene binding. One can see from Table 2 that the binding energies between $3C_{60}$ and Aβ(16-22) octamer for the top six most-populated clusters are varied from -165.4 to -193.4 kcal/mol, while those between C_{180} and Aβ(16-22) octamer are much lower, ranging from -180.3 to 217.2 kcal/mol, indicating stronger binding affinity of C_{180} with Aβ(16-22) octamer than $3C_{60}$, consistent with the interaction energy shown in Fig. 4(b).

Table 2: Binding free energies (ΔG_{bind}, in kcal/mol) of fullerenes ($3C_{60}$ and C_{180}) with Aβ(16-22) octamer for the top six most-populated clusters in Aβ+$3C_{60}$ and Aβ+C_{180} systems at 310 K.

Systems	Clusters	ΔE_{vdW}	ΔG_{GB}	ΔG_{surf}	ΔG_{bind}
Aβ+$3C_{60}$	C1’	-186.0	20.9	-13.7	-178.8 ± 5.5
	C2’	-173.6	21.1	-12.9	-165.4 ± 10.1
	C3’	-190.4	22.4	-14.0	-182.0 ± 6.5
	C4’	-203.4	24.7	-14.7	-193.4 ± 7.6
	C5’	-194.4	23.5	-14.1	-184.9 ± 5.9
	C6’	-198.9	27.6	-14.6	-185.9 ± 10.0
Aβ+C_{180}	C1”	-201.7	26.4	-12.3	-187.6 ± 7.7
	C2”	-225.8	24.3	-12.7	-214.2 ± 5.6
	C3”	-231.5	27.0	-12.6	-217.2 ± 5.1
	C4”	-224.7	24.2	-12.8	-213.3 ± 5.8
	C5”	-194.0	25.8	-12.0	-180.3 ± 11.9
	C6”	-215.1	26.8	-12.8	-201.0 ± 8.9

To further identify which residues are important for the stronger Aβ-C_{180} interactions, we plotted in Fig. 4(c) the interaction energy between each amino acid residue and the three nanoparticles. Consistent with the total fullerene-Aβ interaction energy in Fig. 4(b), we found that the interaction strength of each amino acid residue with C_{180} is larger than that with $3C_{60}$, especially the hydrophobic and aromatic L17-V18-F19-F20 residues. Among all of the residues, Phe at position 19 (F19) has the strongest interaction with fullerenes, with an interaction energy of -5.7 and -6.7 kcal/mol with $3C_{60}$ and C_{180}, respectively. The observation that F20 has slightly lower interaction strength with fullerenes than F19 is probably due to its less hydrophobic environment than F19. Consistently, strong interactions between aromatic residues and carbon nanoparticles were reported in previous experimental and computational studies on the adsorption of amyloid and non-amyloid peptide monomers to the surface of carbon nanoparticles.[56-59] The strong Phe-fullerene interaction would interfere with the Phe-Phe interaction that is important for Aβ(16-22) aggregation, thus weakening the Phe-Phe interaction (Fig. 3(a-b)) and reducing the β-sheet formation probability.

The hexagonal rings of fullerene display better packing with the aromatic rings of Phe residues than the pentagonal rings, resulting in stronger Aβ-C_{180} interactions. To reveal the physical forces underlying the stronger C_{180}-Aβ interaction relative to $3C_{60}$-Aβ interaction, we examine the packing between the aromatic side chains of Phe residues and the carbon rings of fullerenes. Unlike carbon nanotubes or graphenes composed of purely hexagonal (R6) rings, fullerenes consist

of both pentagonal (R5) and hexagonal (R6) rings. For example, a C_{60} molecule contains 20 R6 and 12 R5 rings, while a C_{180} molecule has 80 R6 and 12 R5 rings. The number of R5 rings is a constant of 12, while the number of R6 rings increases with the size of fullerene molecules. The total number of R6 rings is 60 in $3C_{60}$, while it is 80 in C_{180}. We present in Fig. 5(a-c) the PDF of centroid distance (*d*) between the aromatic rings of Phe residues and the R5/R6 rings of C_{60}/$3C_{60}$/C_{180} nanoparticles. We found that in Aβ+C_{60} and Aβ+$3C_{60}$ systems, there exist two peaks centered at 0.45 nm and 0.8 nm, with a dominant peak at 0.45 nm, both for R5 and R6 rings. The dominant peak in Aβ+C_{180} system is shifted to 0.35 nm for Phe-R6 distance and to 0.50 nm for Phe-R5 distance, leading to a dramatic separation of the dominant R5 and R6 peaks. The shift of Phe-R6 distance distribution peak to a shorter distance (0.35 nm) reflects stronger interactions between the aromatic rings of Phe residues and the R6 rings of C_{180} than that with R5 rings, which explains the stronger C_{180}-Aβ interaction relative to $3C_{60}$-Aβ interaction seen in Fig. 4.

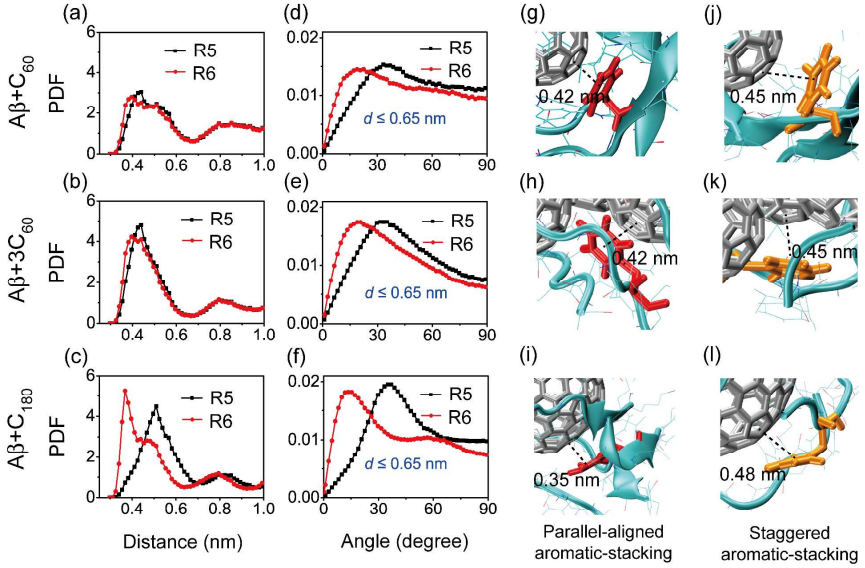

Figure 5: Analysis of aromatic-stacking interactions between the aromatic rings of Phe residues and the pentagonal (R5) and hexagonal (R6) rings of fullerene in Aβ+C_{60}, Aβ+3C_{60} and Aβ+C_{180} systems. The PDF of the centroid distance (*d*) between the aromatic rings of Phe residues (each Phe residue is considered) and its closest carbon rings (R5 and R6) in the three different systems (a-c). The PDF of the angle between the aromatic rings of Phe and the fullerene R5 (black curve) /R6 (red curve) rings with a centroid distance of $d \leq 0.65$ nm in (d) Aβ+C_{60}, (e) Aβ+3C_{60} and (f) Aβ+C_{180} systems. Parallel-aligned (red) (R6-Phe) and staggered (orange) (R5-Phe) aromatic stackings in (g, j) Aβ+C_{60}, (h, k) Aβ+3C_{60} and (i, l) Aβ+C_{180} systems.

We further probe the favorable orientation between the R5/R6 rings of fullerene and the aromatic rings of Phe residues by calculating the PDF of the interplanar ring angle at a centroid distance of $d \leq 0.65$ nm (in Fig. 5(d-f)). In all of the systems, there is one broad peak both for R5-Phe and R6-Phe rings, while the two peaks are located at two different angles. The R5-Phe peak is centered at ~35°, indicating a staggered orientation between the Phe-R5 rings. For the R6-Phe peak, we see a broad peak centered at 15° in Aβ+C_{60} and Aβ+3C_{60} systems and a relatively sharper peak at 10° in Aβ+C_{180} system, implying that the two rings have a strong preference to be parallel-aligned. The smaller angle of 10° between the aromatic rings of Phe residues and the R6 rings of C_{180} reflects stronger aromatic-stacking interactions between these two rings. These results explain why C_{180} has a stronger inhibition effect on the β-sheet formation than 3C_{60}. The parallel-aligned (red, Fig. 5(g-i)) and staggered (orange, Fig. 5(j-l)) aromatic stackings are shown in the representative structures of Aβ+C_{60}, Aβ+3C_{60} and Aβ+C_{180} systems. Perpendicular (T-shaped) ring organizations are also observed in these three systems, but with a much lower probability.

We also calculated the total PDF of the centroid distance (*d*) between the aromatic

rings of Phe and its closest carbon rings (summation of R5 and R6), and the angle between the two rings with a centroid distance of $d \leq 0.65$ nm for the three Aβ-fullerene systems. We see in Fig. S3(a) that the strongest aromatic-stacking interactions are observed between the side chains of Phe and the carbon rings of C_{180}, followed by Phe-3C_{60} and Phe-C_{60} pairs. In addition, parallel-aligned ring geometry is the most favorable one for aromatic-stacking interactions, as seen from the total PDF curve of angle between the aromatic rings of Phe and its closest carbon rings, where a peak appears in the range of 10-20º (Fig. S3(b)). The analysis of aromatic-stacking in a group of non-homologous proteins with known X-ray crystal structures suggests a parallel-displaced aromatic-stacking to be the major organization of aromatic packing in proteins.[60] We note that curvature may also play roles on the inhibitory effect of fullerenes as previous computational studies showed that the carbon nanoparticle's curvature affected the binding affinity of peptide monomers.[57, 61] Smaller curvature of C_{180} may also facilitate the aromatic and hydrophobic residues to bind by providing an effective surface area. Note that we haven't performed the AFM measurements on C_{180} fullerenes as currently it is hard for us to get the C_{180} samples. From the consistency of the AFM results with simulation results on the inhibition effect of C_{60} on Aβ, the stronger inhibition effect of C_{180} obtained from our REMD simulations is reasonable. However, this remains to be investigated.

Carbon nanotubes are composed of purely R6 rings. The influence of single-walled carbon nanotube (SWCNT) (3,3) on the aggregation of Aβ(16-22) octamer was investigated in our previous REMD study and strong inhibition of β-sheet formation

was observed (the average β-sheet content was reduced to 7.9 %).[36] The SWCNT used in that study has a larger curvature than C_{180} and has approximately the same number of carbon atom as C_{180}. The SWCNT contains 102 hexagonal rings, while the C_{180} consists of 80 rings. The SWCNT's stronger inhibition effect on Aβ(16-22) β-sheet formation than C_{180} supports our finding that hexagonal rings play an significant role on the inhibition of β-sheet formation.

As Aβ(16-22) is essential to the fibrillation of full-length Aβ, the inhibition effect of fullerenes on the β-sheet formation of Aβ(16-22) peptides suggest that fullerene may be an efficient inhibitor to retard Aβ40/42 fibrillation by prolonging the lag time for Aβ nucleation. This is supported by a previous experimental study showing that fullerene strongly inhibits Aβ40 aggregation at the early stage by specifically binding to the KLVFF motif.[8] It should be noted that the biological toxicity of pristine fullerenes can be reduced by covalent or non-covalent modifications in the future application. The influence of carbon nanotubes (CNTs) on the fibrillation of other proteins was also studied previously. Linse et al.[10] reported that CNTs (with a diameter of 6 nm) increased the fibrillation rate of β_2-microglobulin by shortening the lag phase for nucleation. Similarly, the effect of graphene/graphite in promoting the fibrillation of other peptides was also reported by experimental[62, 63] and computational[64, 65] studies. These contradictory effects of carbon nanoparticles on amyloid fibrillation clearly need to be clarified and understood.

4. CONCLUSIONS

We have investigated the effect of C_{60} and C_{180} nanoparticles on the β-sheet formation

of Aβ(16-22) peptide by performing three 200-ns atomistic REMD simulations starting from random states. Our REMD simulations combined with AFM images collectively demonstrate that C_{60} nanoparticle at high fullerene concentration (with a C_{60}:Aβ molar ration greater than 1:8) can greatly prevent β-sheet formation. Strikingly, our simulation results show that fullerene C_{180}, with an identical number of carbon atoms as $3C_{60}$ and smaller surface area than $3C_{60}$, has an unexpected stronger inhibitory effect on Aβ(16-22) β-sheet formation. Analysis of the Aβ-fullerene interaction reveals the significant role of fullerene hexagonal rings on the strong inhibitory effect of C_{180}. These results provide novel insight into the inhibition mechanism of fullerenes against the aggregation of Aβ(16-22) and Aβ peptides.

ASSOCIATED CONTENT

Supporting Information. This material includes the description of REMD simulations, analysis parameters, and AFM imaging of Aβ(16-22) aggregation with and without C_{60} nanoparticle, and three figures. The figures show the initial states, the convergence check for all the REMD runs, the PDF of the centroid distance (d) between the aromatic rings of Phe and its closest carbon ring, and the PDF of the angle between the two rings with a centroid distance of $d \leq 0.65$ nm.

AUTHOR INFORMATION

Corresponding Author

*E-mail: ghwei@fudan.edu.cn.

Notes

The authors declare no competing financial interest.

ACKNOWLEDGMENTS

We thank Drs. Ruhong Zhou and Buyong Ma for helpful discussion. This work was supported by the National Science Foundation of China (Grant No.: 91227102 and 11274075). Simulations were performed at the National High Performance Computing Center of Fudan University.

REFERENCES

1. S. Nie, Y. Xing, G. J. Kim and J. W. Simons, *Annu. Rev. Biomed. Eng.*, 2007, **9**, 257-288.
2. J. Klein, *Proc. Natl. Acad. Sci. U. S. A.*, 2007, **104**, 2029-2030.
3. N. L. Rosi, D. A. Giljohann, C. S. Thaxton, A. K. Lytton-Jean, M. S. Han and C. A. Mirkin, *Science*, 2006, **312**, 1027-1030.
4. X. Michalet, F. Pinaud, L. Bentolila, J. Tsay, S. Doose, J. Li, G. Sundaresan, A. Wu, S. Gambhir and S. Weiss, *Science*, 2005, **307**, 538-544.
5. X. Wang, L. Yang, Z. G. Chen and D. M. Shin, *CA. Cancer J. Clin.*, 2008, **58**, 97-110.
6. H. Li, J. Huang, J. Lv, H. An, X. Zhang, Z. Zhang, C. Fan and J. Hu, *Angew. Chem., Int. Ed.*, 2005, **44**, 5100-5103.
7. V. L. Colvin and K. M. Kulinowski, *Proc. Natl. Acad. Sci. U. S. A.*, 2007, **104**, 8679-8680.
8. J. E. Kim and M. Lee, *Biochem. Biophys. Res. Commun.*, 2003, **303**, 576-579.
9. A. V. Ghule, K. M. Kathir, T. K. Suresh Kumar, S.-H. Tzing, J.-Y. Chang, C. Yu and Y.-C. Ling, *Carbon.*, 2007, **45**, 1586-1589.
10. S. Linse, C. Cabaleiro-Lago, W.-F. Xue, I. Lynch, S. Lindman, E. Thulin, S. E. Radford and K. A. Dawson, *Proc. Natl. Acad. Sci. U. S. A.*, 2007, **104**, 8691-8696.
11. C. Cabaleiro-Lago, F. Quinlan-Pluck, I. Lynch, S. Lindman, A. M. Minogue, E. Thulin, D. M. Walsh, K. A. Dawson and S. Linse, *J. Am. Chem. Soc.*, 2008, **130**, 15437-15443.
12. A. M. Saraiva, I. Cardoso, M. C. Pereira, M. A. Coelho, M. J. Saraiva, H. Möhwald and G. Brezesinski, *Chembiochem.*, 2010, **11**, 1905-1913.
13. Y. H. Liao, Y. J. Chang, Y. Yoshiike, Y. C. Chang and Y. R. Chen, *Small*, 2012, **8**, 3631-3639.
14. Y. D. Álvarez, J. A. Fauerbach, J. V. Pellegrotti, T. M. Jovin, E. A. Jares-Erijman and F. D. Stefani, *Nano Lett.*, 2013, **13**, 6156-6163.
15. Q. Ma, G. Wei and X. Yang, *Nanoscale.*, 2013, **5**, 10397-10403.
16. H. Lee, Y. Kim, A. Park and J. M. Nam, *Small*, 2014.
17. S. I. Yoo, M. Yang, J. R. Brender, V. Subramanian, K. Sun, N. E. Joo, S. H. Jeong, A. Ramamoorthy and N. A. Kotov, *Angew. Chem., Int. Ed.*, 2011, **50**, 5110-5115.
18. C. Li and R. Mezzenga, *Nanoscale.*, 2013, **5**, 6207-6218.
19. M. Mahmoudi, H. R. Kalhor, S. Laurent and I. Lynch, *Nanoscale.*, 2013, **5**, 2570-2588.

20. M. Pitschke, R. Prior, M. Haupt and D. Riesner, *Nat. Med.*, 1998, **4**, 832-834.
21. L. C. Serpell, M. Sunde, M. D. Benson, G. A. Tennent, M. B. Pepys and P. E. Fraser, *J. Mol. Biol.*, 2000, **300**, 1033-1039.
22. T. Lührs, C. Ritter, M. Adrian, D. Riek-Loher, B. Bohrmann, H. Döbeli, D. Schubert and R. Riek, *Proc. Natl. Acad. Sci. U. S. A.*, 2005, **102**, 17342-17347.
23. A. T. Petkova, W.-M. Yau and R. Tycko, *Biochemistry.*, 2006, **45**, 498-512.
24. M. A. Grant, N. D. Lazo, A. Lomakin, M. M. Condron, H. Arai, G. Yamin, A. C. Rigby and D. B. Teplow, *Proc. Natl. Acad. Sci. U. S. A.*, 2007, **104**, 16522-16527.
25. D. M. Walsh, I. Klyubin, J. V. Fadeeva, W. K. Cullen, R. Anwyl, M. S. Wolfe, M. J. Rowan and D. J. Selkoe, *Nature*, 2002, **416**, 535-539.
26. S. Lesné, M. T. Koh, L. Kotilinek, R. Kayed, C. G. Glabe, A. Yang, M. Gallagher and K. H. Ashe, *Nature*, 2006, **440**, 352-357.
27. I. Podolski, Z. Podlubnaya, E. Kosenko, E. Mugantseva, E. Makarova, L. Marsagishvili, M. Shpagina, Y. Kaminsky, G. Andrievsky and V. Klochkov, *J. Nanosci. Nanotechnol.*, 2007, **7**, 4-5.
28. E. Makarova, R. Gordon and I. Podolski, *J. Nanosci. Nanotechnol.*, 2012, **12**, 119-126.
29. L. Marsagishvili, A. Bobylev, M. Shpagina, P. Troshin and Z. Podlubnaya, *Biophysics*, 2009, **54**, 135-138.
30. A. Bobylev, L. Marsagishvili and Z. Podlubnaya, *Biophysics*, 2010, **55**, 699-702.
31. A. Bobylev, A. Kornev, L. Bobyleva, M. Shpagina, I. Fadeeva, R. Fadeev, D. Deryabin, J. Balzarini, P. Troshin and Z. Podlubnaya, *Org. Biomol. Chem.*, 2011, **9**, 5714-5719.
32. S. A. Andujar, F. Lugli, S. Höfinger, R. D. Enriz and F. Zerbetto, *Phys. Chem. Chem. Phys.*, 2012, **14**, 8599-8607.
33. C. Hilbich, B. Kisters-Woike, J. Reed, C. L. Masters and K. Beyreuther, *J. Mol. Biol.*, 1992, **228**, 460-473.
34. J. J. Balbach, Y. Ishii, O. N. Antzutkin, R. D. Leapman, N. W. Rizzo, F. Dyda, J. Reed and R. Tycko, *Biochemistry.*, 2000, **39**, 13748-13759.
35. U. F. Röhrig, A. Laio, N. Tantalo, M. Parrinello and R. Petronzio, *Biophys. J.*, 2006, **91**, 3217-3229.
36. H. Li, Y. Luo, P. Derreumaux and G. Wei, *Biophys. J.*, 2011, **101**, 2267-2276.
37. H. Berendsen, J. Postma, W. Van Gunsteren and J. Hermans, *Intermol. forces.*, 1981, **11**, 331-342.
38. Y. Sugita and Y. Okamoto, *Chem. Phys. Lett.*, 1999, **314**, 141-151.
39. H. J. Berendsen, D. van der Spoel and R. van Drunen, *Comput. Phys. Commun.*, 1995, **91**, 43-56.
40. E. Lindahl, B. Hess and D. Van Der Spoel, *J. Mol. Model.*, 2001, **7**, 306-317.
41. W. F. van Gunsteren, S. R. Billeter, A. A. Eising, P. H. Hünenberger, P. Krüger, A. E. Mark, W. R. Scott and I. G. Tironi, 1996.
42. P. H. Nguyen, M. S. Li, G. Stock, J. E. Straub and D. Thirumalai, *Proc. Natl. Acad. Sci. U. S. A.*, 2007, **104**, 111-116.
43. M. G. Krone, L. Hua, P. Soto, R. Zhou, B. Berne and J.-E. Shea, *J. Am. Chem. Soc.*, 2008, **130**, 11066-11072.
44. L. Xie, Y. Luo and G. Wei, *J. Phys. Chem. B*, 2013, **117**, 10149-10160.
45. Z. Fu, Y. Luo, P. Derreumaux and G. Wei, *Biophys. J.*, 2009, **97**, 1795-1803.

46. W. Humphrey, A. Dalke and K. Schulten, *J. Mol. Graph.*, 1996, **14**, 33-38.
47. D. Case, T. Darden, T. Cheatham III, C. Simmerling, J. Wang, R. Duke, R. Luo, R. Walker, W. Zhang and K. Merz, *University of California, San Francisco*, 2012.
48. A. Onufriev, D. Bashford and D. A. Case, *J. Phys. Chem. B*, 2000, **104**, 3712-3720.
49. Q. Wang, X. Yu, K. Patal, R. Hu, S. Chuang, G. Zhang and J. Zheng, *ACS Chem. Neurosci.*, 2013, **4**, 1004-1015.
50. T. Zhang, J. Zhang, P. Derreumaux and Y. Mu, *J. Phys. Chem. B*, 2013, **117**, 3993-4002.
51. W. M. Berhanu and U. H. Hansmann, *Proteins.*, 2013, **81**, 1542-1555.
52. A. D. Williams, E. Portelius, I. Kheterpal, J.-t. Guo, K. D. Cook, Y. Xu and R. Wetzel, *J. Mol. Biol.*, 2004, **335**, 833-842.
53. H. Inouye, K. A. Gleason, D. Zhang, S. M. Decatur and D. A. Kirschner, *Proteins: Struct., Funct., Bioinf.*, 2010, **78**, 2306-2321.
54. M. A. Findeis, G. M. Musso, C. C. Arico-Muendel, H. W. Benjamin, A. M. Hundal, J.-J. Lee, J. Chin, M. Kelley, J. Wakefield and N. J. Hayward, *Biochemistry.*, 1999, **38**, 6791-6800.
55. C. Soto, E. M. Sigurdsson, L. Morelli, R. A. Kumar, E. M. Castaño and B. Frangione, *Nat. Med.*, 1998, **4**, 822-826.
56. G. Zuo, Q. Huang, G. Wei, R. Zhou and H. Fang, *ACS Nano*, 2010, **4**, 7508-7514.
57. G. Zuo, X. Zhou, Q. Huang, H. Fang and R. Zhou, *J. Phys. Chem. C*, 2011, **115**, 23323-23328.
58. A. K. Jana and N. Sengupta, *Biophys. J.*, 2012, **102**, 1889-1896.
59. A. K. Jana, J. C. Jose and N. Sengupta, *Phys. Chem. Chem. Phys.*, 2013, **15**, 837-844.
60. G. B. McGaughey, M. Gagné and A. K. Rappé, *J. Biol. Chem.*, 1998, **273**, 15458-15463.
61. N. Todorova, A. J. Makarucha, N. D. Hine, A. A. Mostofi and I. Yarovsky, *PLoS Comput. Biol.*, 2013, **9**, e1003360.
62. D. Losic, L. L. Martin, M. I. Aguilar and D. H. Small, *Pept. Sci.*, 2006, **84**, 519-526.
63. X. Mao, Y. Wang, L. Liu, L. Niu, Y. Yang and C. Wang, *Langmuir.*, 2009, **25**, 8849-8853.
64. L. Ou, Y. Luo and G. Wei, *J. Phys. Chem. B*, 2011, **115**, 9813-9822.
65. X. Yu, Q. Wang, Y. Lin, J. Zhao, C. Zhao and J. Zheng, *Langmuir.*, 2012, **28**, 6595-6605.

Table of Contents Graphic